Atmos. Chem. Phys. Discuss., 12, 479–523, 2012
www.atmos-chem-phys-discuss.net/12/479/2012/
doi:10.5194/acpd-12-479-2012
© Author(s) 2012. CC Attribution 3.0 License.

Atmospheric Chemistry and Physics Discussions

This discussion paper is/has been under review for the journal Atmospheric Chemistry and Physics (ACP). Please refer to the corresponding final paper in ACP if available.

On the uses of a new linear scheme for stratospheric methane in global models: water source, transport tracer and radiative forcing

B. M. Monge-Sanz[1], M. P. Chipperfield[1], A. Untch[2], J.-J. Morcrette[2], A. Rap[1], and A. J. Simmons[2]

[1]Institute for Climate and Atmospheric Science, School of Earth and Environment, University of Leeds, UK
[2]European Centre for Medium-Range Weather Forecasts, Reading, UK

Received: 10 October 2011 – Accepted: 5 November 2011 – Published: 6 January 2012

Correspondence to: B. M. Monge-Sanz (beatriz@env.leeds.ac.uk)

Published by Copernicus Publications on behalf of the European Geosciences Union.

Abstract

A new linear parameterisation for stratospheric methane (CoMeCAT) has been developed and tested. The scheme is derived from a 3-D full chemistry transport model (CTM) and tested within the same chemistry model itself, as well as in an independent general circulation model (GCM). The new CH_4/H_2O scheme is suitable for any global model and here is shown to provide realistic profiles in the 3-D TOMCAT/SLIMCAT CTM and in the ECMWF (European Centre for Medium-Range Weather Forecasts) GCM. Simulation results from the new stratospheric scheme are in good agreement with the full-chemistry CTM CH_4 field and with observations from the Halogen Occultation Experiment (HALOE). The CH_4 scheme has also been used to derive a source for stratospheric water. Stratospheric water increments obtained in this way within the CTM produce vertical and latitudinal H_2O variation in fair agreement with satellite observations. Stratospheric H_2O distributions in the ECMWF GCM present realistic overall features although concentrations are lower than in the CTM run (up to 0.5 ppmv lower above 10 hPa). The potential of the new CoMeCAT scheme for evaluating long-term transport within the ECMWF model is exploited to assess the impacts of nudging the free running GCM to ERA-40 and ERA-Interim reanalyses. In this case, the nudged GCM shows similar transport patterns to the CTM forced by the corresponding reanalysis data, ERA-Interim producing better results than ERA-40. The impact that the new methane description has in the GCM radiation scheme is also explored. Compared to the default CH_4 climatology used by the ECMWF model, CoMeCAT produces up to 2 K cooling in the tropical lower stratosphere. The effect of using the CoMeCAT scheme for radiative forcing (RF) calculations has been investigated using the off-line Edwards-Slingo (E-S) radiative transfer model. Compared to the use of a tropospheric global 3-D CH_4 value, the CoMeCAT distributions produce an overall decrease in the annual mean net RF, with the largest decrease found over the Southern Hemisphere high latitudes. The effect of the new CH_4 stratospheric distribution on these RF calculations is of up to 30 mW m^{-2}, i.e. the same order of magnitude, and opposite sign, as the inclusion of aircraft contrails formation in the radiative model.

ACPD
12, 479–523, 2012

1 Introduction

Numerical weather prediction (NWP) models and data assimilation systems (DAS) routinely assimilate satellite radiances (e.g. Saunders et al., 1999; McNally et al., 2006), for which a realistic description of stratospheric radiatively active gases is essential. Full chemistry calculations are prohibitively expensive at the resolutions used by NWP/DAS models for operational weather forecasting, and these models must therefore include simplified parameterisations of the species most relevant to them, i.e. greenhouse gases (GHGs) such as O_3, H_2O, CH_4 and chlorofluorocarbons (CFCs). However, the description of these gases is, in many cases, still too simple for current stratospheric purposes.

Water vapour in the stratosphere is not only a radiatively active constituent but is also key for many physical and chemical processes, e.g. polar stratospheric cloud (PSC) formation, liquid aerosol composition and production of the OH radical. Still, stratospheric H_2O vapour simulations within 3-D global models are problematic due to the variety of processes involved. The distribution of water vapour in the stratosphere is the result of a combination of factors: Humidity entry rate through the tropical tropopause layer (TTL), oxidation of CH_4 in the stratosphere, mesospheric photolysis, transport and mixing within the stratosphere and exchange processes through the tropopause. These processes also depend on others, e.g. tropospheric entry rate depends mainly on convection and tropopause temperatures. In addition, feedbacks exist between all the above factors, e.g. radiation, stratospheric circulation and tropical tropopause temperatures. An accurate simulation of stratospheric water vapour is therefore a complicated task that requires different aspects of the DAS/NWP model to interact with a similar accuracy so that larger biases in one factor are not detrimental for the others.

Implementing an H_2O parameterisation simple enough for forecasting purposes, while considering all the relevant processes in an accurate way is not straightforward. One of the current problems is the poor representation of CH_4 found in most general circulation models (GCMs) which, in spite of being a major GHG, is often represented

ACPD
12, 479–523, 2012

as a simply globally averaged value. This is of relevance for H_2O as the main source of stratospheric H_2O is the oxidation of methane (e.g. Bates and Nicolet, 1950; Jones and Pyle, 1984; Le Texier et al., 1988). In a global model the total hydrogen amount $\mathcal{H}$

$$\mathcal{H} = H_2O + 2 \cdot CH_4 + H_2CO + H_2 \quad (1)$$

must be conserved under mixing and transport. More recent studies have shown that the quantity $\mathcal{H}$ is also uniformly distributed in the stratosphere when the last two terms are neglected, i.e. the last two terms are small (e.g. Randel et al., 2004). Austin et al. (2007) confirmed that this is true within 0.05 ppmv[1] precision, which is beyond the precision of available measurements of stratospheric H_2O and CH_4. Methane has no sources in the stratosphere, apart from the entry through the tropopause, and its oxidation results in the production of H_2O. Therefore, a realistic representation of CH_4 is crucial to correctly parameterise a source of stratospheric H_2O.

A few approaches exist for the parameterisation of water vapour in the stratosphere (Dethof, 2003; MacKenzie and Harwood, 2004; Austin et al., 2007; McCormack et al., 2008) but, as discussed in the rest of this section, there are issues they still do not solve. Among such issues are the lack of a realistic latitudinal variability (Dethof, 2003), and the lack of an interactive link between CH_4 and H_2O (McCormack et al., 2008). Also, most of the models used to obtain these parameterisations were two-dimensional therefore, missing the influence of longitudinal features. The exception is the scheme proposed by Austin et al. (2007) which, as discussed below in more detail, overcomes these problems but requires tracers (e.g. an age-of-air tracer) that are not usually available in NWP and DAS models.

The current European Centre for Medium-Range Weather Forecasts (ECMWF) model includes a simple parameterisation of stratospheric water vapour based on the oxidation of CH_4. The current scheme also includes a sink term representing the photolysis of H_2O in the mesosphere. At the basis of such scheme is the observational

[1] parts per million by volume

ACPD
12, 479–523, 2012

evidence that the following quantity is fairly uniformly distributed in the stratosphere with a value of ∼6.8 ppmv (Randel et al., 2004)

$$2[CH_4] + [H_2O] \tag{2}$$

where [ ] stands for volume mixing ratio (vmr). The ECMWF model assumes, therefore, that the vmr of water vapour $[H_2O]$ increases at a rate

$$2k_1[CH_4] \tag{3}$$

or by using Eq. (2),

$$k_1(6.8 - [H_2O]) \tag{4}$$

which is expressed in ppmv and can also be written in terms of specific humidity, q, by simply dividing by 1.6×10^6 as

$$k_1(Q - q) \tag{5}$$

where $Q = 4.25 \times 10^{-6}$ (kg/kg). In addition, above approximately 60 km a term for the H_2O loss by photolysis has to be added, and so the complete ECMWF humidity parameterisation is

$$k_1(Q - q) - k_2 q \tag{6}$$

The rate k_1 can be determined from a model with detailed CH_4 chemistry, such as was done in the past with the 2D-model of the University of Edinburgh (B. Harwood, personal communication, 2004). Nevertheless, a simpler option is used at present by ECMWF, where analytical forms for k_1 and k_2 as a function of pressure are used (Dethof, 2003).

ACPD
12, 479–523, 2012

Both k_1 and k_2 are defined using appropriate timescale factors τ_1 and τ_2:

$$k_1 = \frac{1}{86400 \cdot \tau_1} \tag{7}$$

$$k_2 = \frac{1}{86400 \cdot \tau_2} \tag{8}$$

where k_1 and k_2 are given in s^{-1}, and τ_1 and τ_2 in days. τ_1 and τ_2 are functions of pressure so that the photochemical lifetime of water vapour follows that shown in Brasseur and Solomon (1984). There is no latitudinal or seasonal dependency included in the ECMWF scheme, nor any variation in the CH_4 oxidation source (due for instance to increasing tropospheric concentrations of this gas). ECMWF does not assimilate stratospheric humidity data operationally, but uses the background humidity field directly in the analysis. Therefore, it is the model dynamics and physics which shapes the stratospheric humidity, ultimately constrained to observations by the wind and temperature fields (Simmons et al., 1999).

MacKenzie and Harwood (2004) used the Thin Air 2-D photochemical model (Kinnersley and Harwood, 1993) to obtain the rate coefficient k for the pseudo-reaction that groups the whole CH_4 oxidation process described by Le Texier et al. (1988)

$$CH_4 \xrightarrow{k} 2H_2O \tag{9}$$

the rate k was obtained as a function of latitude, altitude and season using the expression

$$k = \frac{1}{2} \frac{d[H_2O]}{dt} \cdot [CH_4] \tag{10}$$

ACPD
12, 479–523, 2012

Austin et al. (2007) studied the evolution of stratospheric H_2O concentrations in a chemistry climate model (CCM) ensemble run from 1960–2005. They examined the H_2O concentrations coming from the CCM photochemistry scheme (via CH_4 oxidation), and concentrations obtained from a parameterisation involving entry rates, CH_4 oxidation and also mean age-of-air, as the amount of CH_4 oxidised depends on the time air masses have spent in the stratosphere. They formulated the water concentration at a stratospheric location $\boldsymbol{x}$ and time t to be

$$H_2O(\boldsymbol{x},t) = A + B \tag{11}$$

where A, the entry term, and B, the methane oxidation term, can be expressed as

$$A = H_2O|_e(t-\gamma) \tag{12a}$$

$$B = 2\cdot[CH_4|_0(t-\gamma) - CH_4(\boldsymbol{x},t)] \tag{12b}$$

with $\gamma = \gamma(\boldsymbol{x},t)$ the mean age-of-air for that particular location, and $H_2O|_e$ the water vapour amount remaining from the H_2O entry. At present, the kind of parameterisation used in Austin et al. (2007) could not be implemented by ECMWF due to the lack of age-of-air and CH_4 tracers in its Integrated Forecasting System (IFS).

Recently McCormack et al. (2008) described a parameterisation for water vapour production and loss to be used in a high altitude NWP/DAS system. Their method is similar to the current ECMWF approach, with the improvement of including latitudinal variation. They wanted to avoid the inclusion of a CH_4 tracer and therefore focused on the parameterisation of H_2O directly and, in a similar way to MacKenzie and Harwood (2004), they obtain the coefficients k_1 and k_2 in Eq. (6) with a 2-D photochemical model as function of altitude, latitude and season. The main advantage of the scheme

ACPD
12, 479–523, 2012

in McCormack et al. (2008) is its high altitude range, however their study was mainly concerned with the mesospheric region (10–0.001 hPa) and provides no comparative results for our stratospheric study.

Unlike McCormack et al. (2008) and MacKenzie and Harwood (2004), in which a 2-D model was used, we use a 3-D chemistry-transport model (CTM). The linear scheme we present in this paper also differs from that in McCormack et al. (2008) in the conceptual approach of the parameterisation, as ours focuses on parameterising CH_4 in the stratosphere and then using it to obtain a source of stratospheric water vapour. In this way our new scheme provides not only stratospheric H_2O increments but also a realistic CH_4 tracer for the global GCM. Therefore, the new method we propose has the advantage of providing a consistent stratospheric parameterisation of both CH_4 and H_2O, two major GHGs which have the potential to improve the assimilation of radiances in a data assimilation system (DAS), as well as to provide a realistic CH_4 tracer suitable for internal transport checks in the GCM. The new scheme, which has been called CoMeCAT (Coefficients for Methane from a Chemistry And Transport model) can be implemented within any global model and has been here tested within the TOMCAT/SLIMCAT CTM (Chipperfield, 2006) and the ECMWF GCM.

Section 2 in this paper presents the new linear approach used to parameterise CH_4 and H_2O in the stratosphere, while the calculation of the linear coefficients is explained in Sect. 3. The observations used for validation are introduced in Sect. 4. Then results from the new scheme within the CTM simulations are presented, for both methane and water, in Sect. 5 and, correspondingly, Sect. 6 shows the results from the ECMWF GCM simulations. Off-line radiative forcing calculations are discussed in Sect. 7 and the summary and conclusions from the paper are in Sect. 8.

2 Linear approach for methane

Methane is produced at the Earth's surface through human and natural activities, and transported into the stratosphere mainly through the tropical tropopause. CH_4 in the

ACPD
12, 479–523, 2012

stratosphere is only destroyed by oxidation, therefore, the time tendency of stratospheric CH_4 due to chemistry corresponds to

$$\frac{\partial[CH_4]}{\partial t} = -L[CH_4] \tag{13}$$

where [ ] indicates concentrations and L is the CH_4 loss rate (s^{-1}).

Loss of CH_4 in the stratosphere takes place mainly through the following reactions

$$CH_4 + OH \rightarrow CH_3 + H_2O \tag{14a}$$

$$CH_4 + O(^1D) \rightarrow CH_3 + OH \tag{14b}$$

$$CH_4 + Cl \rightarrow CH_3 + HCl \tag{14c}$$

Based on such reactions, the oxidation rate of CH_4 can be written as

$$L = k_1[OH] + k_2[O(^1D)] + k_3[Cl] \tag{15}$$

where the rate constants k_i (i=1, 2, 3) are given in (cm^3 $molecule^{-1} s^{-1}$).

Full chemistry 3-D models such as SLIMCAT calculate the oxidation rate in Eq. (15) analytically from the involved reactions. However, in order to provide NWP models with a simplified methane scheme, an alternative approach has been explored here. As CH_4 is only destroyed, our new scheme parameterises the loss rate L. Since the three reactions involved in CH_4 destruction depend on temperature (T) and [CH_4], L can be parameterised following a scheme similar to the one proposed for the ozone tendency by Cariolle and Déqué (Cariolle and Déqué, 1986; Cariolle and Teyssèdre, 2007):

$$L(CH_4, T) = c_0 + c_1([CH_4] - \overline{[CH_4]}) + c_2(T - \overline{T}) \tag{16}$$

ACPD
12, 479–523, 2012

In this case the coefficients c_i are

$$c_0 = L_0$$
$$c_1 = \left.\frac{\partial L}{\partial [CH_4]}\right|_0 \quad (17)$$
$$c_2 = \left.\frac{\partial L}{\partial T}\right|_0$$

L_0 is the loss rate for a given reference state (subscript 0 indicates values obtained at a reference state), c_1 represents how the loss rate adjusts with changes in the CH_4 concentration, while c_2 relates to how L varies with temperature.

2.1 Scheme for water vapour

Since CH_4 has no stratospheric source except entry through the tropopause, the CoMeCAT CH_4 scheme presented above can also be used to obtain H_2O tendencies in the stratosphere. Based on an approximation of Eq. (1) where the last two terms have been neglected, the time tendency for water vapour in the stratosphere can be written as

$$\frac{\partial [H_2O]}{\partial t} = -2\frac{\partial [CH_4]}{\partial t} \quad (18)$$

We have implemented such scheme in TOMCAT/SLIMCAT 3-D runs, and ECMWF GCM runs, where CH_4 has been parameterised following the CoMeCAT approach and compared to H_2O observations (see Sect. 5.2).

ACPD
12, 479–523, 2012

3 CoMeCAT coefficients

3.1 Calculation methodology

CoMeCAT coefficients have been calculated from full-chemistry runs of the global 3-D TOMCAT/SLIMCAT CTM, similar to the method employed in Monge-Sanz et al. (2011) for the calculation of coefficients for a stratospheric ozone scheme. To calculate the coefficients, the TOMCAT box model was initialised with the zonally averaged output of a full-chemistry simulation of the SLIMCAT 3-D model (Chipperfield, 2006) run 323. Run 323 is a multiannual SLIMCAT run that uses a $7.5^{\circ} \times 7.5^{\circ}$ horizontal resolution and 24 vertical levels (L24). The run is driven by ERA-40 winds (Uppala et al., 2005) from 1977–2001 and by ECMWF operational winds from 2002–2006. The box model configuration is identical to the 3-D CTM (chemical descriptions, resolution etc.) but it does not consider transport processes. The period chosen to initialise the box model corresponds to January to December 2004. From the initial state five 2-day runs of the box model were carried out; one control run and four perturbation runs from the initial conditions. In these runs the chemistry was computed every 20 min. The resolution adopted for the box model is 24 latitudes, and 24 levels (from the surface up to ~60 km), matching the resolution of the full-chemistry run used for the initialisation. The box model also uses the same chemistry module as the full SLIMCAT model.

The reference loss rate L_0 (coefficient c_0), is obtained from a control run in which the zonal 3-D output is used without alteration to initialise the box model. The loss rate is calculated from the three chemical reactions in Eq. (14). The reference state values of $\overline{[CH_4]}$ and $\overline{T}$ are directly provided by the zonal output of the SLIMCAT initial state on the 15th of each month. Then, perturbed runs of the box model are carried out to obtain the coefficients c_1 and c_2. To obtain c_1, variations in $[CH_4]$ of ± 5 % with respect to the reference state are introduced; and variations of ± 4 K to obtain c_2. Further details on the runs used to calculate the coefficients can be found in Monge-Sanz (2008). The calculation results in a set of coefficients for each latitude, level and month of the year.

ACPD
12, 479–523, 2012

The coefficients and climatologies are provided as 5 look-up tables (c_0, c_1, c_2, $\overline{[CH_4]}$ and $\overline{T}$) for every month.

3.2 The new CH_4 coefficients

Figure 1 plots the zonal mean of the reference values for $\overline{[CH_4]}$ and $\overline{T}$ for January and July. Stratospheric CH_4 in the full-chemistry SLIMCAT has been widely validated, and compares very well with MIPAS observations (e.g. Kouker, 2005). The temperature field corresponds to ECMWF operational data for 2004 interpolated onto the CTM grid.

The CoMeCAT zonal mean CH_4 lifetime, τ, is plotted in Fig. 2 for January, April, July and October. The minimum lifetime values are reached at ~1 hPa and are almost 1 yr over the summer pole, region where the maximum CH_4 loss rate takes place. Above 1 hPa, CH_4 loss decreases (lifetime increases) due to the decrease in the abundance of OH. The lifetime values in Fig. 2 are in overall agreement with those in Brasseur and Solomon (2005).

Methane time tendency is controlled mainly by the first coefficient c_0 and the other terms add corrections due to changes in CH_4 and temperature. Figure 3 shows the impact that changes in CH_4 concentrations have on the loss rate (coefficient c_1) for the months of January, April, July and October. Similarly, Fig. 4 shows how temperature changes feedback on the loss rate. Note that the minus sign in Eq. (13) has been included when calculating the coefficients c_i, so the scheme actually parameterises $L' = -L$. In the middle stratosphere, an increase in CH_4 concentration causes a decrease in loss rate L (Fig. 3), explained by the fact that a CH_4 increase implies a decrease of ClO at around 40 km and an overall decrease of HO_x, which leads to a decrease in CH_4 loss. The opposite effect occurs in the LS region and above the stratopause, where a CH_4 increase causes an increased loss rate.

The values of c_2 (loss tendency with respect to temperature) are negative everywhere except in the equatorial LS (between 100–200 hPa) and in the Arctic summer LS (Fig. 4). The negative sign agrees with the fact that by increasing temperature, k_i

ACPD
12, 479–523, 2012

in Eq. (15) increases, which means more CH_4 loss. The decrease in loss over the Arctic summer (positive contours in Fig. 4c) is explained by a secondary effect, coming from decreased OH concentrations at higher temperature, that outweighs the direct temperature effect in this region.

4 HALOE observations of CH_4 and H_2O

The results of the model simulations have been validated against observations from the Halogen Occultation Experiment (HALOE) instrument, on board the Upper Atmosphere Research Satellite (UARS, Russell et al., 1993) of CH_4 (Park et al., 1996) and H_2O (Harries et al., 1996). The HALOE data used in our study correspond to the third public release v19 (W. Randel and F. Wu, personal communication, 2007). These HALOE data are zonally averaged and are available for 41 latitudes (80°N-80°S), and 49 pressure levels (from 100–0.01 hPa); the monthly time series covers the period November 1991 – November 2005. The accuracy for these CH_4 observations is better than 7 % between 1–100 hPa (Park et al., 1996) and 10 % for H_2O measurements at the same altitude range. Such HALOE data have been widely validated and have been used for several model results validations (e.g. Chipperfield et al., 2002; Bregman et al., 2006; Eyring et al., 2006; Feng et al., 2007).

5 CoMeCAT in the SLIMCAT CTM

Table 1 describes the 3-D CTM runs that have been performed using ERA-40 winds (Uppala et al., 2005) and ERA-Interim winds (Dee et al., 2011). Two SLIMCAT-mode (with hybrid σ-θ vertical levels) runs driven by ERA-40 winds, one implementing the CoMeCAT scheme for CH_4 (run13) and one full-chemistry (run323). Also two TOMCAT-mode (σ-p vertical coordinate) runs, both implementing the CoMeCAT scheme, one driven by ERA-40 and the other by ERA-Interim winds. The CH_4 tracer in these 3-D

ACPD
12, 479–523, 2012

CTM runs was initialised with the concentrations from the reference climatology $[\overline{CH_4}]$. The same climatology was used to overwrite the tracer value at the surface at every time step, to prevent the surface values from drifting during the model simulations. The initial values for the H_2O tracer were $7.0\times10^{-6} - 2[\overline{CH_4}]$.

5.1 CoMeCAT against full-chemistry

5.1.1 Methane cross-sections

Figure 5 shows the annual mean zonal average CH_4 concentrations from the parameterisation in run13, as well as differences with the full-chemistry run323 and with HALOE CH_4 measurements above 100 hPa. Results in Fig. 5 correspond to year 2000; which is different from the year used to compute the CoMeCAT coefficients, calculated for the meteorological conditions of 2004 (Sect. 3). Both simulations, CoMeCAT and full-chemistry used the same ECMWF ERA-40 winds. The CoMeCAT parameterisation is able to capture all general features and variability. There are differences over the tropics above 10 hPa, where CoMeCAT CH_4 concentrations are slightly smaller (up to 0.05 ppmv), as well as in LS high latitudes, where CoMeCAT simulates up to 0.10 ppmv more than SLIMCAT full-chemistry over the Arctic. The overall agreement with HALOE is good; modelled concentrations, both CoMeCAT and full-chemistry, are up to 0.20 ppmv lower than HALOE in the most upper levels (above 20 hPa) in the SH, with maximum differences concentrated around 10 hPa at high latitudes in both hemispheres. CoMeCAT simulates more CH_4 than observed over the tropical mid-stratosphere and most upper levels at high NH latitudes. The differences between the two modelled CH_4 fields (CoMeCAT and full-chemistry) are smaller than the differences between the modelled fields and HALOE observations.

ACPD
12, 479–523, 2012

5.1.2 Methane vertical profiles

Annual averaged (year 2000) vertical distributions from CoMeCAT and the full-chemistry run 323 between 100–0.2 hPa are shown in Fig. 6, for five different latitudes. The CoMeCAT vertical distribution in the SLIMCAT run (run13) agrees well with the full chemistry run. The most significant differences occur above 1 hPa, where CoMeCAT overestimates CH_4 by up to 0.1 ppmv, and below 30 hPa, where the parameterisation, especially at southern midlatitudes, results in smaller concentrations than the full-chemistry (up to 0.05 ppmv smaller). CoMeCAT in the TOMCAT run (run14) is also in good agreement with full-chemistry in the LS, but in the middle and upper stratosphere it simulates more CH_4 than the SLIMCAT run13. Above 1.0 hPa differences of up to 0.25 ppmv widely occur and run14 results in up to 0.40 ppmv more than run323 in the highest levels at tropical latitudes, the reason for these differences being the too fast vertical transport in the TOMCAT-mode run (Monge-Sanz et al., 2007).

5.2 CoMeCAT water distributions within the CTM

To obtain CoMeCAT water distributions with the SLIMCAT CTM, the humidity field from the ECMWF analysis is used in the troposphere, while in the stratosphere the relation described in Eq. (18) is used to obtain H_2O tendencies from CoMeCAT. We define the tropopause differently in the tropics and outside the tropical region. In the tropics (15° S–15° N) it is defined as the level at which the minimum temperature is reached, while outside the tropics the stratospheric water scheme is used when the absolute potential vorticity (PV) is larger than 2 PVU[2] and the potential temperature (θ) larger than 380 K, or if θ >300 K.

Figure 7 shows water vertical profiles for the 2000 annual average from CoMeCAT along with HALOE observations. The overall variability is well captured by the CoMeCAT approach, the best agreement is found over NH high and mid latitudes. In the LS

[2]PVU is *potential vorticity unit* and its value is: 1PVU= 10^{-6} m^2 s^{-1} K kg^{-1}.

ACPD
12, 479–523, 2012

CoMeCAT shows a wet bias of ∼0.6 ppmv in the range 100–50 hPa, then agreement in the middle stratosphere (50–3 hPa) is very good for all latitudes, except over southern high latitudes where CoMeCAT H_2O is between 0.2–0.8 ppmv larger than observed by HALOE. Above 3 hPa, CoMeCAT again produces larger concentrations (0.2–0.5 ppmv) than observed. The discrepancy over southern high latitudes between CoMeCAT and HALOE in the LS is most probably due to the lack of Antarctic dehydration in the CoMeCAT scheme.

6 CoMeCAT CH_4 in the ECMWF GCM

A series of runs within the ECMWF GCM (IFS) have been carried out using the CoMeCAT scheme to parameterise stratospheric CH_4 and H_2O. The runs were performed with the Cy36r1 model version (operational in 2010) with a resolution of T159L60. Table 2 describes the runs carried out with this model to examine the ability of CoMeCAT to reproduce CH_4 and H_2O in the ECMWF model. One additional ECMWF run was performed to evaluate the impact of CoMeCAT on the ECMWF radiation scheme (Sect. 6.2).

6.1 ECMWF CoMeCAT CH_4 distributions

The ECMWF runs were initialised with the same CH_4 reference field as the CTM runs. Figure 6 shows annually averaged CH_4 vertical distributions from the CoMeCAT scheme in the CTM and in the ECMWF GCM (run fif4). Two different CTM runs have been included, the default SLIMCAT ($\sigma-\theta$) one (run13) and also one TOMCAT ($\sigma-p$) run (run14) for a better comparison against the ECMWF runs, which, like the GCM, also uses a $\sigma-p$ vertical coordinate. The overall agreement in the LS (up to 10 hPa) is good between all runs and observations (with differences smaller than 0.1 ppmv), larger differences occur above 10 hPa. At the highest levels the agreement with observations is good for fif4 and SLIMCAT run13 in Fig. 6, also within 0.1 ppmv difference.

ACPD
12, 479–523, 2012

Between 1–10 hPa the ECMWF CoMeCAT run (fif4) simulates smaller concentrations than the full-chemistry (by up to 0.2 ppmv) at high and midlatitudes in the NH; while in the SH the underestimation (up to 0.3 ppmv) takes place between 5–50 hPa. Over the tropics the ECMWF run is very close to the SLIMCAT runs in the LS and middle stratosphere. This, together with the fact that in the upper levels fif4 is more realistic than TOMCAT forced by ERA-40 winds, shows the improvement in the vertical transport achieved in the recent ECMWF model versions (e.g. Monge-Sanz et al., 2007; Dee et al., 2011). Nevertheless, definitive conclusions cannot be drawn on this issue since the vertical motion used in the model runs is different: the CTM obtains it from the divergence of the horizontal winds, while the ECMWF runs use the instantaneous vertical wind velocity w. The ECMWF w field had been reported to be too noisy in the past (e.g. Fueglistaler et al., 2004; Krüger et al., 2008; Tegtmeier et al., 2008), while more recent studies point to a significant noise reduction (e.g. Liu et al., 2010; Ploeger et al., 2011), in agreement with our comparison in Fig. 6.

6.2 Impact on the ECMWF stratospheric temperature

Methane is a strong greenhouse gas that warms the troposphere and middle/lower stratosphere, and cools the mesosphere/upper stratosphere. Despite this, most GCMs use only a fixed constant value for CH_4 concentrations (e.g. Collins et al., 2006); i.e. these models consider CH_4 as a well-mixed gas, which is unrealistic above the tropopause. Using a simpler parameterisation approach than CoMeCAT, Curry et al. (2006) showed the impact that relaxing the well-mixed approximation for some greenhouse gases (GHGs) had in the stratosphere. They used the Canadian AGCM3 general circulation model (McFarlane et al., 1992) with a simplified treatment for the chemical loss of N_2O, CH_4, CFC-11 and CFC-12. They found a general cooling of the stratosphere compared to the use of well-mixed concentrations for these GHGs, mainly caused by the additional H_2O resulting from the CH_4 oxidation. Curry et al. (2006) also found increases in temperature in the upper winter stratosphere, of up to 8 K over the pole.

ACPD
12, 479–523, 2012

In past versions of the IFS GCM a global CH_4 value of 1.72 ppmv was used by the ECMWF radiation scheme (Bechtold et al., 2009), such value is typical of tropospheric levels and was shown by Monge-Sanz (2008) to cause temperature biases in the upper stratosphere compared to the use of the CoMeCAT tracer coupled to the ECMWF radiation scheme. In the IFS version used in the present study, the default CH_4 field included in the radiation scheme is a two-dimensional climatology derived from the reanalysis of the Global and regional Earth-system Monitoring using Satellite and in-situ data project (GEMS, Hollingsworth et al., 2008).

In order to evaluate the impact that CoMeCAT has on the ECMWF temperature field, compared to the new default climatology, CoMeCAT has been made interactive with the ECMWF radiation scheme, and temperature changes in the GCM have been examined. For this, the IFS run fipj has been carried out, in which the CoMeCAT CH_4 field, instead of the default GEMS climatology, is coupled to the GCM radiation scheme. This GCM run is a 1-yr forecast with an additional spin-up period of 2 months. The length of the run allows us to examine temperature differences in the mid-upper stratosphere in the summer hemisphere, and in the tropical UTLS region. However, the dynamical variability can be too large in winter high latitudes, as well as in low tropospheric levels, to determine temperature differences here.

Figure 8 shows the June-July-August (JJA) averaged differences in temperature in the ECMWF model using the default operational ECMWF CH_4 climatology (run fif4) in the IFS radiation scheme and using the CH_4 distributions from the CoMeCAT tracer (run fipj). Absorption by CH_4 is considered both in the shortwave (SW) and the long-wave (LW) in the two runs. With CoMeCAT, temperature decreases appear over the tropics (between 20° N–20° S) between 10–100 hPa; temperature values in this region are up to 2.0 K lower than with the IFS default climatology. The temperature changes observed over the winter hemisphere cannot be related to CH_4 as dynamical winter variability between the two compared runs can be larger than changes induced by different CH_4 distributions. Differences in the CH_4 fields of both runs (fipj-fif4) are shown in Fig. 9. The largest CH_4 differences (up to 0.50 ppmv) over mid and high latitudes

ACPD
12, 479–523, 2012

are found between 10–100 hPa, while over the tropics the largest differences (up to 0.35 ppmv) appear above 10 hPa. The match between these CH_4 differences and the temperature differences in Fig. 8 is not straightforward. The largest effects on temperature may appear above the tropical tropopause because for this region the overall radiative heating rate is at a relative minimum and also the vertical gradient in CH_4 is most significant.

6.3 Nudging effects and transport

The use of nudged GCMs is increasing over recent years as a potential way to make these models closer to the real atmosphere (Jeuken et al., 1996; Schmidt et al., 2006; Telford et al., 2008; Douville, 2009). Such an approach consists of relaxing, or nudging, the GCM dynamical fields towards meteorological (re)analyses, so that, if M is the model operator and G the nudging parameter, the evolution of a certain model variable $\boldsymbol{x}$ is given by

$$\frac{\partial \boldsymbol{x}}{\partial t} = M(\boldsymbol{x} + G(\boldsymbol{x}_{an} - \boldsymbol{x})) \tag{19}$$

Nudging will improve temperature and fast horizontal wind fields; however, the impact of nudging on the slow stratospheric meridional circulation needs to be tested with a suitable tracer. Here we have explored the effect that nudging the ECMWF GCM has for the transport of the CoMeCAT CH_4 tracer. The experiments fh22 and fh23 (Table 2) have been produced with the same GCM version and the same CoMeCAT parameterisation as the run fi6n, however, in fh22 the dynamical variables are relaxed to ERA-40 values (year 2000) and to ERA-Interim in fh23. The relaxation is done instantaneously every 6 h.

The CoMeCAT CH_4 scheme has provided the GCM with a tracer that can be used for the on-line evaluation of long-term transport effects. Here we have used this tracer to assess the effect that nudging has on stratospheric transport of tracers compared to

ACPD
12, 479–523, 2012

the free-running GCM, to our knowledge this is the first time this kind of evaluation has been done.

Figure 10 shows CoMeCAT CH_4 annually averaged cross-sections for the free-running experiment fi6n, the nudged runs fh22 and fh23, the CoMeCAT-SLIMCAT run13 and the CoMeCAT-TOMCAT run14 and run15 (Table 1). Compared to the free-running fi6n, fh22 results in larger CH_4 concentrations at almost all levels and latitudes. At the upper most levels (above 1 hPa) the GCM run nudged to ERA-40 produces between 0.2 ppmv (at high latitudes) and 0.3 ppmv (at the tropics) more than fi6n. This is similar to the effect observed when running CoMeCAT in the TOMCAT ($\sigma - p$) run forced by ERA-40 (Fig. 10c), compared to the SLIMCAT run (Fig. 10a). These too high CH_4 values in the upper stratosphere are related to the excessive vertical transport exhibited by ERA-40 in TOMCAT simulations, see e.g. Monge-Sanz et al. (2007). Therefore, our results suggest that nudging is bringing the GCM closer to the transport features in ERA-40, with the associated known problems.

The TOMCAT run forced by ERA-Interim brings the CH_4 distribution closer to that from the SLIMCAT run. Similarly, the GCM run nudged to ERA-Interim (fh23) is in better agreement with the free-running GCM than fh22. This indicates that the effect the too fast stratospheric transport in ERA-40 had on stratospheric tracers is significantly improved in ERA-Interim.

Thus, in a nudged GCM, an upper limit to the quality of the dynamical fields is set by the meteorological data used for the nudging. When ERA-40 fields are used, the nudged GCM shows the same problems as the off-line CTM driven by the same ERA-40 fields, while the distribution of the stratospheric tracers also improves in a similar way in the TOMCAT ERA-Interim run and in the GCM nudged to ERA-Interim fields.

6.4 CoMeCAT water in the GCM

The ECMWF default (currently operational) stratospheric water scheme, and H_2O obtained from the CoMeCAT CH_4 in the ECMWF runs have been compared against HALOE observations and H_2O from CoMeCAT in the CTM. Figure 11 shows H_2O

ACPD
12, 479–523, 2012

cross-sections averaged over 2000 obtained from CoMeCAT in the CTM and in the ECMWF model (run fi6n). Also shown in the same figure are H_2O from the default ECMWF scheme (run fif4), and from an ECMWF control run (fif5) in which no water source scheme is used in the stratosphere. The ECMWF runs are initialised with the same initial conditions as the CTM CoMeCAT for H_2O, i.e. $7.0 \times 10^{-6} - 2[\overline{CH_4}]$.

6.4.1 ECMWF default H_2O scheme

The ECMWF stratospheric water currently comes from a parameterisation based on a fixed profile of water vapour observed lifetime (e.g. Dethof, 2003). This scheme does not include any latitudinal variation, relying on the accuracy of the Brewer-Dobson circulation to get the correct amount of H_2O increase in the stratosphere due to CH_4 oxidation. Figure 11d shows H_2O from an ECMWF run (fif4) using this default stratospheric water scheme. At high latitudes in the upper levels (above 5 hPa) fif4 H_2O concentrations are around 0.5 ppmv lower than HALOE. One control run has also been carried out (run fif5) in which the source of water in the stratosphere has been switched off (Fig. 11c). It can be seen that the H_2O field would be far too low in the stratosphere in the absence of a source parameterisation, up to 1.5 ppmv are added by the default ECMWF H_2O scheme which also makes the concentration gradients realistic. Compared to the CTM run and to HALOE observations, the ECMWF H_2O distributions show a negative bias in the tropical LS around 100 hPa; H_2O in the ECMWF run is 2.5 ppmv smaller than in the CTM run (Fig. 11a) and 2.0 ppmv smaller than HALOE observations (Fig. 11e). This bias is present in all three ECMWF simulations, independent of the scheme used to obtain stratospheric H_2O, which indicates a characteristic of this version of the ECMWF GCM that will require further investigation.

6.4.2 ECMWF new H_2O scheme from CoMeCAT

The distribution of water from the CoMeCAT scheme implemented in the ECMWF model (run fi6n) is shown in Fig. 11b. Compared to the performance of the same

ACPD
12, 479–523, 2012

scheme in SLIMCAT (Fig. 11a) the ECMWF run shows lower water values (up to 0.5 ppmv lower above 10 hPa). The SLIMCAT run is closer to the HALOE distribution (Fig. 11e). In the ECMWF model, CoMeCAT produces vertical distributions of H_2O similar to those from the IFS default scheme, except at high levels (above 10 hPa), where CoMeCAT can simulate up to 0.4 ppmv more H_2O at some latitudes (Fig. 7). The differences between the CoMeCAT H_2O distributions in the CTM and the ECMWF runs partly arise from the fact that fi6n comes from the free-running GCM while the SLIMCAT run is forced by 6-hourly ERA-40 analyses. This last factor is conditioning the concentrations entering through the tropopause, it is the analysed humidity field that is adopted for the troposphere in the CTM runs. ERA-40 presents a 10 % wet bias with respect to HALOE in the LS (100 hPa) (Oikonomou and O'Neill, 2006). The too high water values that enter the CoMeCAT scheme from the tropopause are accumulated throughout the entire stratosphere causing the CoMeCAT CTM run to present higher concentrations than HALOE (Fig. 11a). On the other hand, the problems shown by the ECMWF default H_2O scheme in previous analysis versions, e.g. in ERA-40 (Uppala et al., 2005), have been partially overcome due to a more realistic transport in the more recent ECMWF model versions (like the one used for run fif4).

7 Radiative forcing implications

Further calculations of the radiative effect (RE) of the CoMeCAT CH_4 distribution, have been performed with the off-line version of the Edwards-Slingo (E-S) radiative transfer model (Edwards and Slingo, 1996) with a $144 \times 72 \times 23$ (longitude x latitude x altitude) resolution. This radiative model uses 9 bands in the longwave and 6 bands in the shortwave and a delta-Eddington 2 stream scattering solver at all wavelengths. The E-S model employs a monthly averaged climatology based on ERA-40 data for temperature, ozone and water vapour. Monthly mean climatological cloud fields and surface albedo (averaged over the period 1983–2005) are taken from the International Satellite

ACPD
12, 479–523, 2012

Cloud Climatology Project (ISCCP) archive (Rossow and Schiffer, 1999). Clouds are added to three vertical levels, corresponding to low, middle and high clouds.

The CoMeCAT radiative effect has been evaluated for each calendar month by taking the difference between two runs of the radiation code: One "control" run using a global 3-D constant CH_4 value of 1.80 ppmv for CH_4 (the same for every calendar month) and one 'perturbed' run taking the CH_4 distribution from the CoMeCAT CH_4 field in the SLIMCAT run13 (CH_4 monthly means from run13 are provided to the radiation model). The value of 1.80 ppmv is the value used by the CoMeCAT runs in the troposphere. In this way, with these two runs of the E-S model, we can evaluate RE differences due only to stratospheric CH_4.

Figure 12 shows the annual mean values of the net RE differences, at the tropopause after allowing for stratospheric adjustment, between the 'perturbed' and the 'control' radiation runs. Changing from the constant 1.80 ppmv value used in the control run to the much more realistic distribution in the stratosphere results in global cooling; negative differences are found in all regions, with a global average value of $-11.0\,\mathrm{mW\,m^{-2}}$. These differences are of the same order of magnitude as those obtained when including aircraft contrails formation in the radiative model (Rap et al., 2010). The smallest differences in Fig. 12 are found over the tropics (20° N–20° S), and the largest over Antarctica.

These results imply that RE calculations using a well-mixed approximation that overestimates stratospheric methane concentrations will overestimate surface warming globally. However, a cautionary note has to be made here: our RE calculations do not take into account that the reduction in stratospheric CH_4 should be accompanied by an increase in the source of stratospheric water vapour. That extra water vapour will act on RE calculations in the opposite sense, i.e. cooling the stratosphere and warming the surface levels. Since our two runs of the E-S use the same ERA-40 climatology the effect of the associated H_2O increments are missed in our comparison. On the other hand, the ERA-40 climatology used here for the E-S runs is known to be too dry in the stratosphere (e.g. Uppala et al., 2005), which means that E-S runs with a more realistic

ACPD
12, 479–523, 2012

field of stratospheric H_2O (e.g. from ERA-Interim) would produce a larger warming effect, coming from stratospheric H_2O, than that obtained with the present version of the E-S model. This remains as a future line of research.

The effect due to larger water vapour concentrations would partly compensate the differences shown in Fig. 12. Nevertheless, the inclusion of realistic profiles for other GHGs, like N_2O and CFCs, is expected to have a similar effect to the one we have shown here for methane. Although beyond the scope of this paper, future research should be done on the effects that realistic GHGs vertical distributions in the stratosphere have for radiative forcing calculations and, therefore, climate studies.

8 Conclusions

A new CH_4 parameterisation scheme (CoMeCAT) has been developed for the stratosphere, and tested within a 3-D CTM and a 3-D GCM. The scheme has also been used to parameterise stratospheric water vapour in the two 3-D models. The adaptability of the scheme to different conditions has been proved by showing results for atmospheric conditions differing from those used to calculate the scheme coefficients (conditions for year 2004 were used to obtain the coefficients).

The CoMeCAT CH_4 performs well in the TOMCAT/SLIMCAT CTM, showing very good agreement with observations from HALOE and with CTM full-chemistry runs. The largest differences with observations are found at high latitudes, especially in the SH, where CoMeCAT (and full-chemistry) runs with ERA-40 underestimate CH_4 compared to HALOE, by up to 0.3 ppmv at altitudes around 10 hPa. CoMeCAT also performs well in the ECMWF GCM, producing realistic CH_4 distributions. When running CoMeCAT interactively with the GCM radiation scheme, the new CH_4 in the ECMWF model cools the tropical LS region (up to 2 K) compared to the use of the default GEMS CH_4 climatology.

The inclusion of CoMeCAT in the ECMWF model allows the possibility of exploring long-term transport features in the GCM. In particular, we have used CoMeCAT

ACPD
12, 479–523, 2012

to evaluate a nudged version of the GCM, and to compare the performance of ERA-Interim and ERA-40 to transport the stratospheric tracer. Nudging the GCM to ERA-40 analyses produced similar CH_4 distributions to those obtained with TOMCAT (σ-p) run by ERA-40. Nudging the GCM to ERA-Interim brought about improvements, compared to the nudging to ERA-40, similar to those obtained in the TOMCAT run driven by ERA-Interim fields. These results indicate that a nudged GCM incorporates the advantages and deficiencies of the analyses used, and nudging a recent version of the ECMWF IFS to ERA-40 is not recommended, at least for applications involving transport of stratospheric tracers.

The CH_4 time tendency obtained from CoMeCAT has been used in both models (CTM and GCM) to parameterise the source of stratospheric water. The H_2O distributions obtained from CoMeCAT in the CTM runs are in good agreement with HALOE observations, except for a wet bias in the LS region of ~0.6 ppmv. This is at least partly due to the use of ERA-40 humidity values in the troposphere, which present a wet bias at the tropopause. In the ECMWF model the CoMeCAT water approach performs well. ECMWF CoMeCAT H_2O distributions show a realistic spatial variability and good agreement with HALOE observations, except for a dry bias in the tropical lower stratosphere (of up to 2.0 ppmv).

The CoMeCAT scheme is a more realistic treatment for stratospheric CH_4 than previously included in ECMWF. Improving the representation of greenhouse gases in the stratosphere was initially tested in the ECMWF IFS (Monge-Sanz, 2008; Bechtold et al., 2009), and shown to reduce temperature biases in the stratosphere. As a next step, the effect of using CoMeCAT in conjunction with similar schemes for other GHGs in IFS should be investigated; implementing schemes similar to CoMeCAT for other radiatively active gases like N_2O and CFCs would also improve the representation of the stratosphere in the ECMWF GCM. In addition, including this type of methane scheme in the ECMWF model would also enable the assimilation of CH_4 concentrations to be used to constrain humidity analyses in the stratosphere.

ACPD
12, 479–523, 2012

The CoMeCAT scheme also opens new possibilities for climate studies. In spite of being the second most important greenhouse gas, most climate models use only a fixed value for CH_4 in the stratosphere. Including a realistic CH_4 profile, with latitude dependence and linked to other model variables (like temperature), is expected to produce changes to radiative forcing results in climate models. In our study, including the CoMeCAT methane distribution in the off-line Edwards-Slingo (E-S) radiation model has an effect on the calculated radiative forcing values of the same order of magnitude, but of different sign, as the incorporation of aircraft contrail formation. The use of CoMeCAT instead of a well-mixed approximation in the stratosphere has reduced radiative forcing values by up to 30 mW m^{-2} over mid and high latitudes, with a global annually averaged decrease of −11.0 mW m^{-2}. This implies that a realistic representation of vertical distribution of GHGs in the stratosphere is necessary to better constrain radiative forcing and climate warming projections. In this sense it can be said that the stratosphere plays a similar role to that played by the oceans: the stratosphere acts as a slow evolving boundary for the troposphere, and a realistic description of stratospheric processes is key to increase the accuracy of long-term climate predictions. In addition, Solomon et al. (2010) highlighted the need for better representations of stratospheric H_2O in climate models to better simulate and interpret decadal surface warming trends; the CoMeCAT scheme could also contribute in this respect.

Acknowledgements. We thank Elias Hólm for valuable communications on the ECMWF H_2O scheme and Piers Forster for helpful discussions on the interaction of the scheme with the GCM radiation. This work has been partially funded by the NERC Research Award NE/F004575/1 and the EU GEOMON project.

References

Austin, J., Wilson, J., Li, F., and Vömel, H.: Evolution of Water Vapor Concentrations and Stratospheric Age of Air in Coupled Chemistry-Climate Model Simulations, J. Atmos. Sci., 64, 905–921, doi:10.1175/JAS3866.1, 2007. 482, 485

ACPD
12, 479–523, 2012

Bates, D. R. and Nicolet, M.: The photochemistry of water vapour, J. Geophys. Res., 55, 301–327, 1950. 482

Bechtold, P., Orr, A., Morcrette, J.-J., Engelen, R., Flemming, J., and Janiskova, M.: Improvements in the stratosphere and mesosphere of the IFS, ECMWF Newsletter, 2009. 496, 503

Brasseur, G. and Solomon, S.: Aeronomy of the Middle Atmosphere, D. Reidel Publishing, Co. Dordrecht, 1984. 484

Brasseur, G. and Solomon, S.: Aeronomy of the Middle Atmosphere, Springer, Dordrecht, 2005. 490

Bregman, B., Meijer, E., and Scheele, R.: Key aspects of stratospheric tracer modeling using assimilated winds, Atmos. Chem. Phys., 6, 4529–4543, doi:10.5194/acp-6-4529-2006, 2006. 491

Cariolle, D. and Déqué, M.: Southern Hemisphere Medium-Scale Waves and Total Ozone Disturbances in a Spectral General Circulation Model, J. Geophys. Res., 91, 10825–10846, 1986. 487

Cariolle, D. and Teyssèdre, H.: A revised linear ozone photochemistry parameterization for use in transport and general circulation models: multi-annual simulations, Atmos. Chem. Phys., 7, 2183–2196, doi:10.5194/acp-7-2183-2007, 2007. 487

Chipperfield, M. P.: New version of the TOMCAT/SLIMCAT off-line chemical transport model, Q. J. R. Meteorol. Soc., 132, 1179–1203, doi:0.1256/qj.05.51, 2006. 486, 489

Chipperfield, M. P., Khattatov, B. V., and Lary, D. J.: Sequential assimilation of stratospheric chemical observations in a three-dimensional model, J. Geophys. Res., 107, doi:10.1029/2002JD002110, 2002. 491

Collins, W., Ramaswamy, V., Schwarzkopf, M., Sun, Y., Portmann, R., Fu, Q., Casanova, S., Dufresne, J.-L., Fillmore, D., Forster, P., Galin, V., Gohar, L., Ingram, W., Kratz, D., Lefebvre, M.-P., Li, J., Marquet, P., Oinas, V., Tsushima, Y., Uchiyama, T., and Zhong, W.: Radiative forcing by well-mixed greenhouse gases: Estimates from climate models in the Intergovernmental Panel on Climate Change (IPCC) Fourth Assessment Report (AR4), J. Geophys. Res., 111, doi:10.1029/2005JD006713, 2006. 495

Curry, C. L., McFarlane, N. A., and Scinocca, J. F.: Relaxing the well-mixed greenhouse gas approximation in climate simulations: Consequences for stratospheric climate, J. Geophys. Res., 111, doi:10.1029/2005JD006670, 2006. 495

Dee, D. P., Uppala, S. M., Simmons, A. J., Berrisford, P., Poli, P., Kobayashi, S., Andrae, U., Balmaseda, M. A., Balsamo, G., Bauer, P., Bechtold, P., Beljaars, A. C. M., van de Berg, L.,

ACPD
12, 479–523, 2012

Bidlot, J., Bormann, N., Delsol, C., Dragani, R., Fuentes, M., Geer, A. J., Haimberger, L., Healy, S., Hersbach, H., Hólm, E. V., Isaksen, L., Kållberg, P., Köhler, M., Matricardi, M., McNally, A. P., Monge-Sanz, B. M., Morcrette, J.-J., Peubey, C., de Rosnay, P., Tavolato, C., Thépaut, J.-N., and Vitart, F.: The ERA-Interim reanalysis: Configuration and performance of the data assimilation system, Q. J. R. Meteorol. Soc., 137, 553–597, doi:10.1002/qj.828, 2011. 491, 495

Dethof, A.: Aspects of modelling and assimilation for the stratosphere at ECMWF, SPARC Newsletter, 2003. 482, 483, 499

Douville, H.: Stratospheric polar vortex influence on Northern Hemisphere winter climate variability, Geophys. Res. Lett., 36, doi:10.1029/2009GL039334, 2009. 497

Edwards, J. M. and Slingo, A.: Studies with a flexible new radiation code: I. Choosing a configuration for a large scale model, Q. J. R. Meteorol. Soc., 122, doi:10.1002/qj.49712253107, 689–720, 1996. 500

Eyring, V., Butchart, N., Waugh, D. W., Akiyoshi, H., Austin, J., Bekki, S., Bodeker, G. E., Boville, B. A., Brühl, C., Chipperfield, M. P., Cordero, E., Dameris, M., Deushi, M., Fioletov, V. E., Frith, S. M., Garcia, R. R., Gettelman, A., Giorgetta, M. A., Grewe, V., Jourdain, L., Kinnison, D. E., Mancini, E., Manzini, E., Marchand, M., Marsh, D. R., Nagashima, T., Newman, P. A., Nielsen, J. E., Pawson, S., Pitari, G., Plummer, D. A., Rozanov, E., Schraner, M., Shepherd, T. G., Shibata, K., Stolarski, R. S., Struthers, H., Tian, W., and Yoshiki, M.: Assessment of temperature, trace species, and ozone in chemistry-climate model simulations of the recent past, J. Geophys. Res., 111, doi:10.1029/2006JD007327, 2006. 491

Feng, W., Chipperfield, M. P., Dorf, M., Pfeilsticker, K., and Ricaud, P.: Mid-latitude ozone changes: studies with a 3-D CTM forced by ERA-40 analyses, Atmos. Chem. Phys., 7, 2357–2369, doi:10.5194/acp-7-2357-2007, 2007. 491

Fueglistaler, S., Wernli, H., and Peter, T.: Tropical troposphere-to-stratosphere transport inferred from trajectory calculations, J. Geophys. Res., 109, 16, doi:10.1029/2003JD004069, 2004. 495

Harries, J. E., Russell, J. M., Tuck, A. F., Gordley, L. L., Purcell, P., Stone, K., Bevilacqua, R. M., Gunson, M., Nedoluha, G., and Traub, W. A.: Validation of measurements of water vapor from the Halogen Occultation Experiment (HALOE), J. Geophys. Res., 101, 10205–10216, 1996. 491

Hollingsworth, A., Engelen, R. J., Textor, C., Benedetti, A., Boucher, O., Chevallier, F., Dethof, A., Elbern, H., Eskes, H., Flemming, J., Granier, C., Kaiser, J. W., Morcrette, J.-J., Rayner,

ACPD
12, 479–523, 2012

P. R., Peuch, V.-H., Rouil, L., Schultz, M. G., Simmons, A. J., and the GEMS Consortium: Toward a monitoring and forecasting system for atmospheric composition: the GEMS project., B. Am. Meteor. Soc., 89, 1147–1164, doi:10.1175/2008BAMS2355.1, 2008. 496

Jeuken, A., Siegmund, P., Heijboer, L., Feichter, J., and Bengtsson, L.: On the Potential of assimilating meteorological analyses in a global climate model for the purposes of model validation, J. Geophys. Res., 101, 16939–16950, 1996. 497

Jones, R. L. and Pyle, J. A.: Observations of CH_4 and N_2O by the Nimbus 7 SAMA: A comparison with in situ data and two-dimensional numerical model calculations, J. Geophys. Res., 89, 5263–5279, 1984. 482

Kinnersley, J. S. and Harwood, R. S.: An isentropic two-dimensional model with an interactive parameterization of dynamical and chemical planetary wave fluxes, Q. J. R. Meteorol. Soc., 119, 1167–1193, 1993. 484

Kouker, W.: Towards the Prediction of Stratospheric Ozone (TOPOZ III), Scientific Report. EC Contract EVK2-CT-2001-00102, European Commission, Brussels, Belgium, 2005. 490

Krüger, K., Tegtmeier, S., and Rex, M.: Long-term climatology of air mass transport through the Tropical Tropopause Layer (TTL) during NH winter, Atmos. Chem. Phys., 8, 813–823, doi:10.5194/acp-8-813-2008, 2008. 495

Le Texier, H., Solomon, S., and Garcia, R. R.: The role of molecular hydrogen and methane oxidation in the water vapour budget of the stratosphere, Q. J. R. Meteorol. Soc., 114, 281–295, 1988. 482, 484

Liu, Y. S., Fueglistaler, S., and Haynes, P. H.: Advection-condensation paradigm for stratospheric water vapor, J. Geophys. Res., 115, doi:10.1029/2010JD014352, 2010. 495

MacKenzie, I. A. and Harwood, R. S.: Middle atmospheric response to a future increase in humidity arising from increased methane abundance, J. Geophys. Res., 109, doi:10.1029/2003JD003590, 2004. 482, 484, 485, 486

McCormack, J. P., Hoppel, K. W., and Siskind, D. E.: Parameterization of middle atmospheric water vapor photochemistry for high-altitude NWP and data assimilation, Atmos. Chem. Phys., 8, 7519–7532, doi:10.5194/acp-8-7519-2008, 2008. 482, 485, 486

McFarlane, N. A., Boer, G. J., Blanchet, J.-P., and Lazare, M.: The Canadian Climate Centre second-generation general circulation model and its equilibrium climate, J. Climate, 5, 1013–1044, 1992. 495

McNally, A. P., Watts, P. D., A. Smith, J., Engelen, R., Kelly, G. A., Thépaut, J. N., and Matricardi, M.: The assimilation of AIRS radiance data at ECMWF, Q. J. R. Meteorol. Soc., 132, 935–

ACPD
12, 479–523, 2012

957, doi:10.1256/qj.04.171, 2006. 481
Monge-Sanz, B. M.: Stratospheric transport and chemical parameterisations in ECMWF analyses: evaluation and improvements using a 3D CTM, Ph.D. thesis, School of Earth and Environment, University of Leeds, 2008. 489, 496, 503
Monge-Sanz, B. M., Chipperfield, M. P., Simmons, A. J., and Uppala, S. M.: Mean age of air and transport in a CTM: Comparison of different ECMWF analyses, Geophys. Res. Lett., 34, doi:10.1029/2006GL028515, 2007. 493, 495, 498
Monge-Sanz, B. M., Chipperfield, M. P., Cariolle, D., and Feng, W.: Results from a new linear O3 scheme with embedded heterogeneous chemistry compared with the parent full-chemistry 3-D CTM, Atmos. Chem. Phys., 11, 1227–1242, doi:10.5194/acp-11-1227-2011, 2011. 489
Oikonomou, E. K. and O'Neill, A.: Evaluation of ozone and water vapor fields from the ECMWF reanalysis ERA-40 during 1991-1999 in comparison with UARS satellite and MOZAIC aircraft observations, J. Geophys. Res., 111, doi:10.1029/2004JD005341, 2006. 500
Park, J., Russell, J., L.Gordley, L., Drayson, S. R., Banner, D., McInerney, J., Gunson, M. R., Toon, G., Sen, B., Blavier, J.-F., Webster, C., Zipf, E., Erdman, P., Schmidt, U., and Schiller, C.: Validation of Halogen Occultation Experiment CH_4 measurements from the UARS, J. Geophys. Res., 101, 10217–10240, 1996. 491
Ploeger, F., Fueglistaler, S., Grooß, J.-U., Gnther, G., Konopka, P., Liu, Y. S., Müller, R., Ravegnani, F., Schiller, C., Ulanovski, A., and Riese, M.: Insight from ozone and water vapour on transport in the tropical tropopause layer (TTL), Atmos. Chem. Phys., 11, 407–419, doi:10.5194/acp-11-407-2011, 2011. 495
Randel, W., Wu, F., Oltmans, S. J., Rosenlof, K., and Nedoluha, G. E.: Interannual Changes of Stratospheric Water Vapor and Correlations with Tropical Tropopause Temperatures, J. Atmos. Sci., 61, 2133–2148, 2004. 482, 483
Rap, A., Forster, P. M., Jones, A., Boucher, O., Haywood, J. M., Bellouin, N., and De Leon, R. R.: Parameterization of contrails in the UK Met Office Climate Model, J. Geophys. Res., 115, doi:10.1029/2009JD012443, 2010. 501
Rossow, W. and Schiffer, R.: Advances in understanding clouds from ISCCP, B. Am. Meteorol. Soc., 80, 2261–2288, 1999. 501
Russell, J. M., Gordley, L. L., Park, J. H., Drayson, S. R., Hesketh, W. D., Cicerone, R. J., Tuck, A. F., Frederick, J. E., Harries, J. E., and Crutzen, P. J.: The Halogen Occultation Experiment, J. Geophys. Res., 98, 10777–10797, 1993. 491

ACPD
12, 479–523, 2012

Saunders, R., Matricardi, M., and Brunel, P.: An improved fast radiative transfer model for assimilation of satellite radiance observations, Q. J. R. Meteorol. Soc., 125, 1407–1425, doi:10.1002/qj.1999.49712555,615, 1999. 481

Schmidt, G., Ruedy, R., Hansen, J., Aleinov, I., Bell, N., Bauer, M., Bauer, S., Cairns, B., Canuto, V., Cheng, Y., Del Genio, A., Faluvegi, G., Friend, A., Hall, T., Hu, Y., Kelley, M., Kiang, N., Koch, D., Lacis, A., Lerner, J., Lo, K., Miller, R., Nazarenko, L., Oinas, V., Perlwitz, J., Perlwitz, J., Rind, D., Romanou, A., Russell, G., Sato, M., Shindell, D., Stone, P., Sun, S., Tausnev, N., Thresher, D., and Yao, M.-S.: Present day atmospheric simulations using GISS Model: Comparison to in-situ, satellite and reanalysis data, J. Climate, 19, 153–192, 2006. 497

Simmons, A. J., Untch, A., Jakob, C., Kållberg, P., and Undén, P.: Stratospheric water vapour and tropical tropopause temperatures in ECMWF analyses and multi-year simulations, Q. J. R. Meteorol. Soc., 125, 353–386, 1999. 484

Solomon, S., Rosenlof, K. H., Portmann, R. W., Daniel, J. S., Davis, S. M., Sanford, T. J., and Plattner, G.-K.: Contributions of stratospheric water vapor to decadal changes in the rate of global warming, Science, 327, 1219–1223, 2010. 504

Tegtmeier, S., Krüger, K., Wohltmann, I., Schoellhammer, K., and Rex, M.: Variations of the residual circulation in the Northern Hemispheric winter,, J. Geophys. Res., 113, doi:10.1029/2007JD009518, 2008. 495

Telford, P. J., Braesicke, P., Morgenstern, O., and Pyle, J. A.: Technical Note: Description and assessment of a nudged version of the new dynamics Unified Model, Atmos. Chem. Phys., 8, 1701–1712, doi:10.5194/acp-8-1701-2008, 2008. 497

Uppala, S. M., Kållberg, P. W., Simmons, A. J., Andrae, U., Bechtold, V. D. C., Fiorino, M., Gibson, J. K., Haseler, J., Hernandez, A., Kelly, G. A., Li, X., Onogi, K., Saarinen, S., Sokka, N., Allan, R. P., Andersson, E., Arpe, K., Balmaseda, M. A., Beljaars, A. C. M., Berg, L. V. D., Bidlot, J., Bormann, N., Caires, S., Chevallier, F., Dethof, A., Dragosavac, M., Fisher, M., Fuentes, M., Hagemann, S., Hólm, E., Hoskins, B. J., Isaksen, L., Janssen, P. A. E. M., Jenne, R., McNally, A. P., Mahfouf, J.-F., Morcrette, J.-J., Rayner, N. A., Saunders, R. W., Simon, P., Sterl, A., Trenberth, K. E., Untch, A., Vasiljevic, D., Viterbo, P., and Woollen, J.: The ERA-40 Re-analysis, Q. J. R. Meteorol. Soc., 131, 2961–3012, doi:10.1256/qj.04.176, 2005. 489, 491, 500, 501

ACPD
12, 479–523, 2012

Table 1. TOMCAT/SLIMCAT CTM runs.

CTM run	CTM mode	Winds	CH_4
run13	SLIMCAT	ERA-40	CoMeCAT
run14	TOMCAT	ERA-40	CoMeCAT
run15	TOMCAT	ERA-Interim	CoMeCAT
run323	SLIMCAT	ERA-40	full-chem

ACPD
12, 479–523, 2012

Table 2. ECMWF runs with CoMeCAT CH_4 and H_2O schemes.

ECMWF run	GCM	CH_4 scheme	H_2O scheme
fif4	Free GCM	CoMeCAT	ECMWF default
fi6n	Free GCM	CoMeCAT	CoMeCAT
fif5	Free GCM	none	none
fh22	Nudged to ERA-40 every 6h	CoMeCAT	ECMWF default
fh23	Nudged to ERA-Interim every 6h	CoMeCAT	ECMWF default

ACPD
12, 479–523, 2012

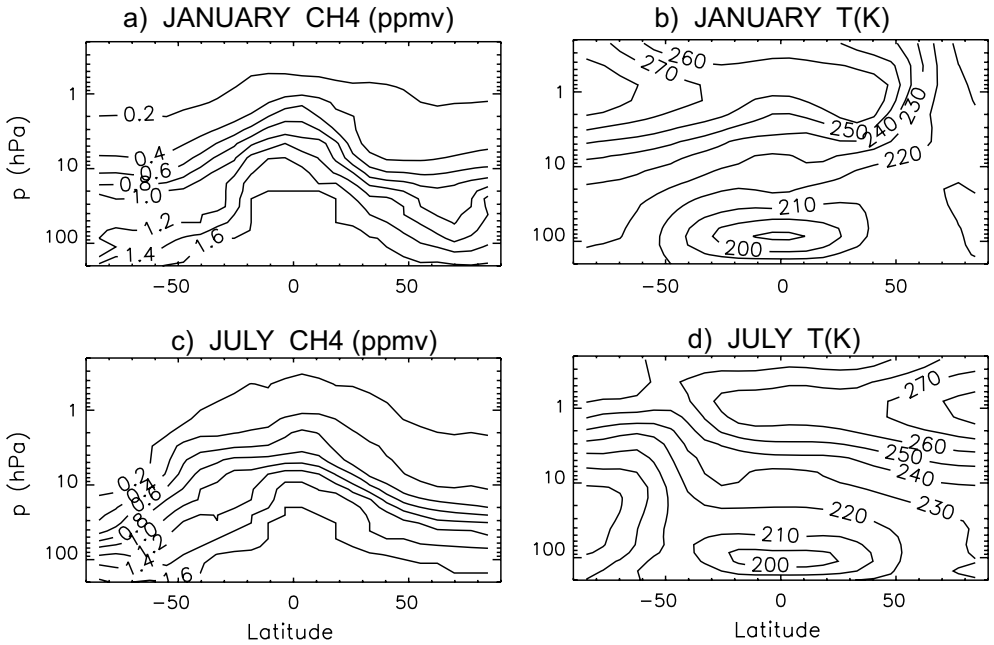

Fig. 1. Zonal mean of CoMeCAT $\overline{[CH_4]}$ (ppmv) (left panels), and temperature (K) (right panels) reference terms for January (top row) and July (bottom row).

ACPD
12, 479–523, 2012

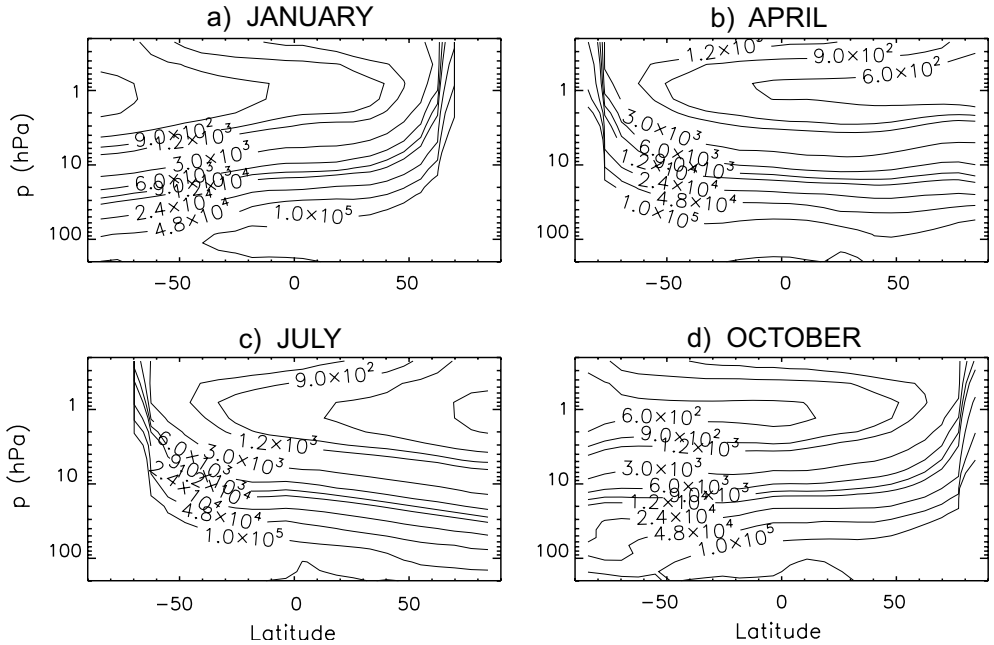

Fig. 2. Altitude/latitude distribution of CoMeCAT CH_4 lifetime values (in days) for **(a)** January, **(b)** April, **(c)** July and **(d)** October.

ACPD
12, 479–523, 2012

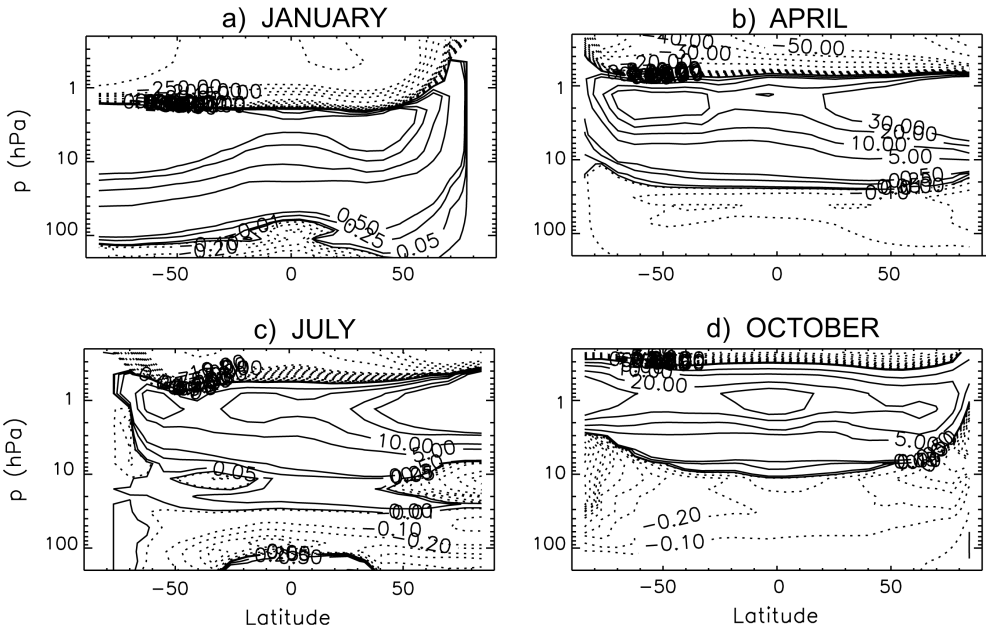

Fig. 3. Altitude/latitude distribution of the CoMeCAT loss tendency with $[CH_4]$ (coefficient c_1) in units of (10^{-14}day^{-1}ppmv^{-1}) for **(a)** January, **(b)** April, **(c)** July and **(d)** October.

ACPD
12, 479–523, 2012

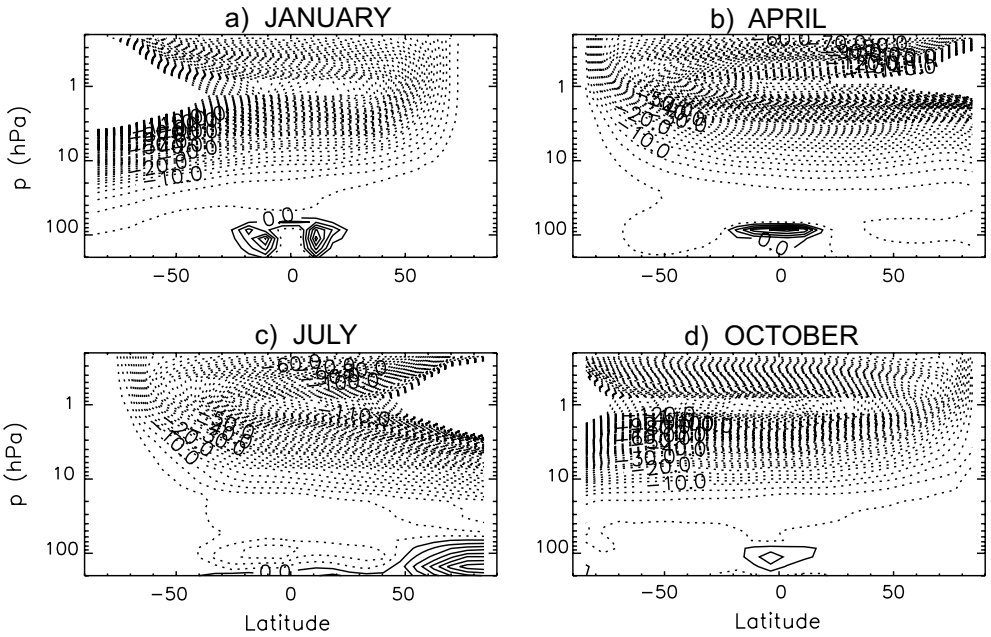

Fig. 4. Altitude/latitude distribution of the CoMeCAT loss tendency with temperature (coefficient c_2) in units of (10^{-16} day^{-1} K^{-1}) for **(a)** January, **(b)** April, **(c)** July and **(d)** October.

ACPD
12, 479–523, 2012

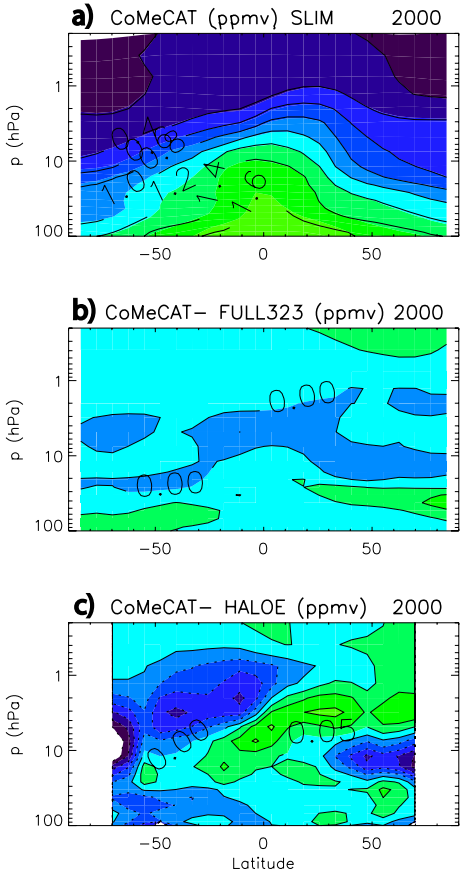

Fig. 5. Annual mean for 2000 of **(a)** zonally averaged CH_4 distribution (ppmv) from the CoMeCAT scheme in the CTM run13, **(b)** differences between CoMeCAT and full-chemistry run of SLIMCAT (run323) and **(c)** differences between CoMeCAT and HALOE observations. The model simulations use ERA-40 winds. Contour values are 0.20 ppmv for **(a)** and 0.05 ppmv for **(b)** and **(c)**. Colour scale in panel **(a)** goes from larger concentrations (darkest green) to smaller concentrations (darkest blue); while for panels **(b)** and **(c)** the colour scale indicates most positive differences (in darkest green) and most negative differences (in darkest blue).

ACPD
12, 479–523, 2012

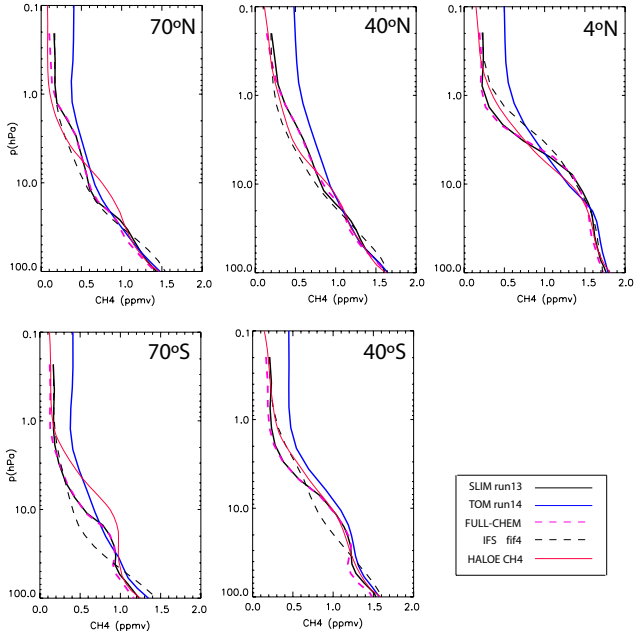

Fig. 6. Annually averaged CH_4 distributions (ppmv) for year 2000 from the CoMeCAT scheme in SLIMCAT run13 (solid black line), TOMCAT run14 (blue line) and in the ECMWF GCM (dashed black line) run fif4 (Table 2) for the latitudes 70° N, 40° N, 4° N, 70° S and 40° S (as labelled). HALOE observations have also been included (solid red line), as well as the CTM full-chemistry run323 (dashed red line).

ACPD
12, 479–523, 2012

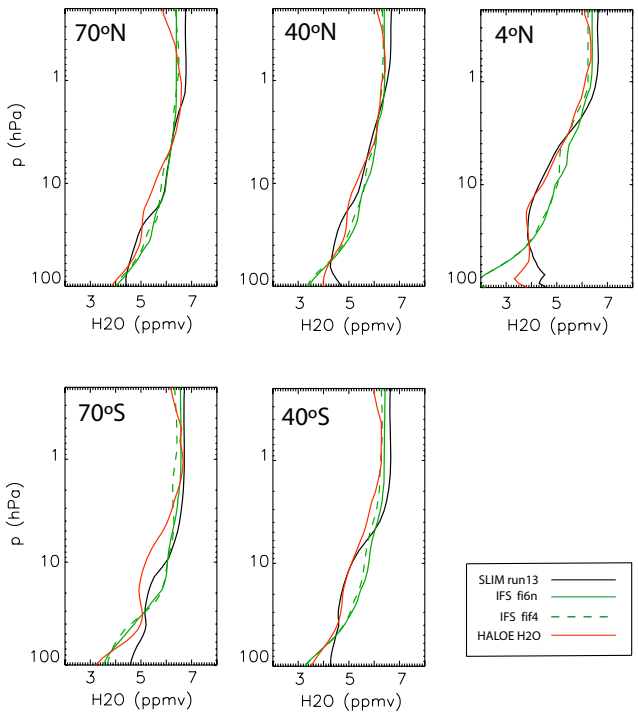

Fig. 7. Annually averaged H_2O distributions (ppmv) for year 2000 from the CoMeCAT scheme in the SLIMCAT run13 (black line), ECMWF default run fif4 (dashed green line), CoMeCAT in ECMWF run fi6n (solid green line) and HALOE observations (red line). Profiles correspond to the latitudes 70° N, 40° N, 4° N, 70° S and 40° S (as labelled).

ACPD
12, 479–523, 2012

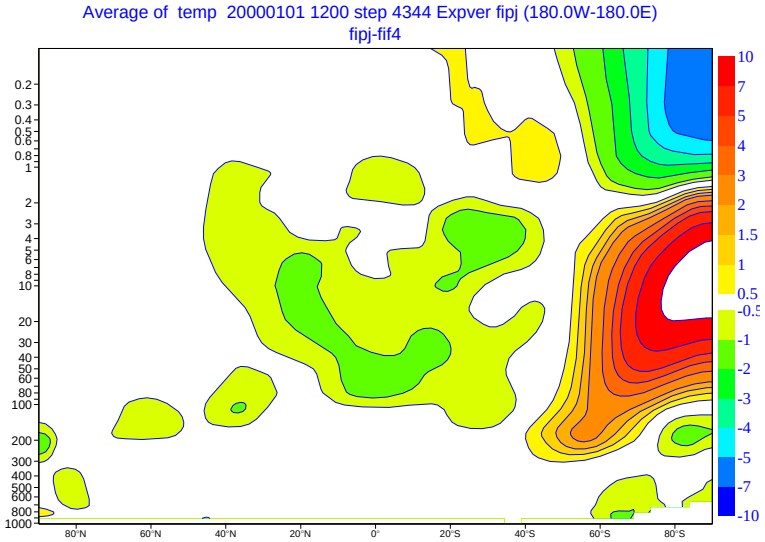

Fig. 8. Differences in temperature, averaged over June-July-August (JJA) 2000, between the ECMWF runs fipj (CoMeCAT CH_4 in the radiation scheme) and run fif4 (GEMS CH_4 climatology in the radiation scheme). Colour scale goes from most negative differences (dark blue) to most positive differences (dark red).

ACPD
12, 479–523, 2012

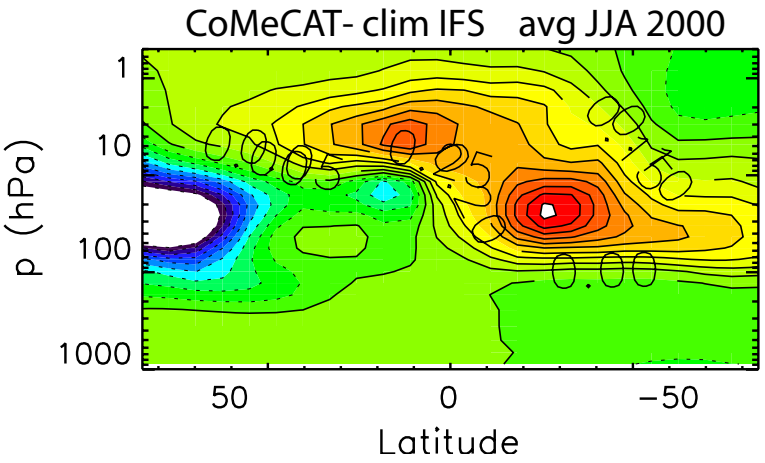

Fig. 9. Differences in the CH_4 concentrations between the CoMeCAT distribution and ECMWF GEMS climatology in the radiation scheme, averaged for June-July-August (JJA) 2000. Colour scale goes from most negative differences (dark blue) to most positive differences (dark red). Contour interval is 0.05 ppmv.

ACPD
12, 479–523, 2012

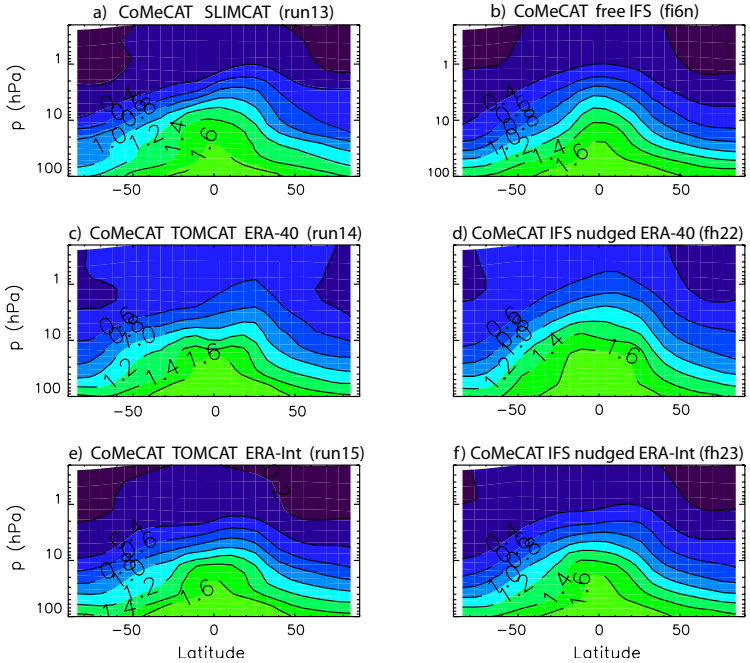

Fig. 10. Annually averaged zonal CH_4 distributions (ppmv) for year 2000 from the CoMeCAT tracer in **(a)** the SLIMCAT CTM run13, **(b)** the free-running GCM fi6n, **(c)** the TOMCAT run14 forced by ERA-40 fields, **(d)** the GCM run fh22 nudged to ERA-40, **(e)** the TOMCAT run15 forced by ERA-Interim and **(f)** the GCM run fh23 nudged to ERA-Interim. Colour scale goes from larger concentrations (dark green) to smaller concentrations (dark blue). Contour interval is 0.20 ppmv.

ACPD
12, 479–523, 2012

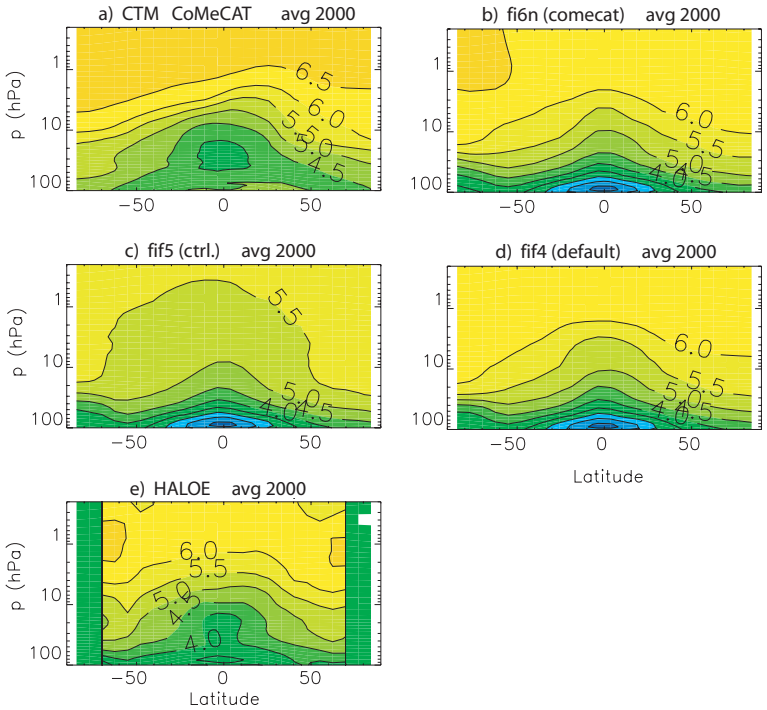

Fig. 11. H_2O (ppmv) cross-sections averaged over 2000 obtained from **(a)** CoMeCAT in the SLIMCAT run13, **(b)** CoMeCAT in ECMWF run fi6n, **(c)** ECMWF control run fif5, **(d)** ECMWF default scheme in run fif4 and **(e)** HALOE instrument. Colour scale goes from larger concentrations (orange) to smaller concentrations (dark blue). Contour interval is 0.5 ppmv.

ACPD
12, 479–523, 2012

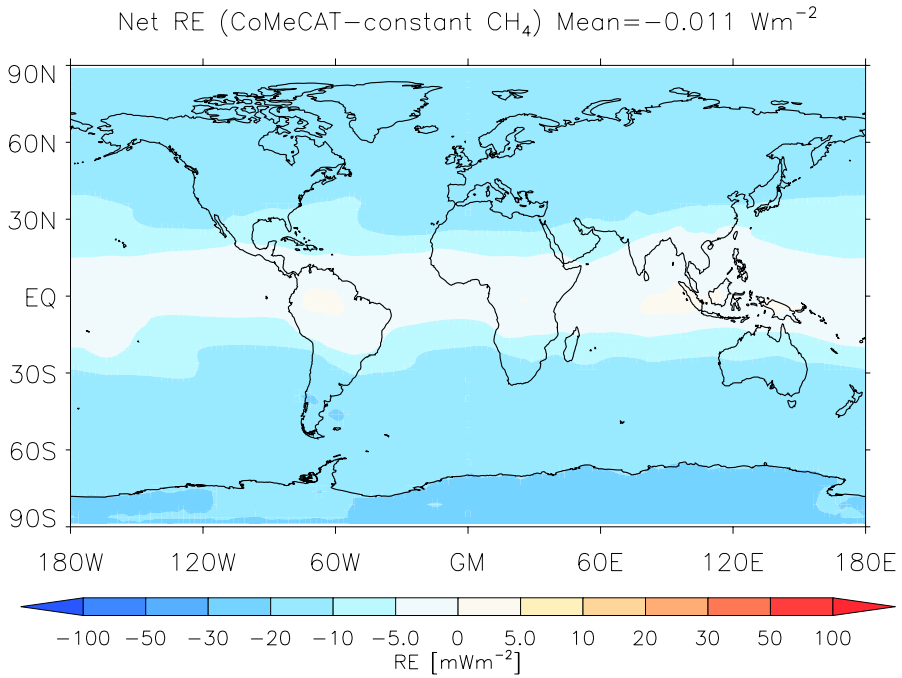

Fig. 12. Annually averaged net radiative forcing ($mW\,m^{-2}$) induced by using the CoMeCAT CH_4 instead of a default constant value of 1.80 ppmv in the Edwards-Slingo radiation model (see Sect. 7 for details). In the colour scale, blue is for negative radiative effect (cooling) and red for positive radiative effect (warming). The effect of the new CH_4 scheme is, therefore, a general annual average cooling, with the strongest effect (up to $-30\,mW\,m^{-2}$) found over high latitudes.

ACPD
12, 479–523, 2012